

Spin-active single photon emitters in hexagonal boron nitride from carbon-based defects

Fernanda Pinilla, Nicolás Vásquez, and Ignacio Chacón

Departamento de Física, Facultad de Ciencias, Universidad de Chile. Santiago, Chile

Jerónimo R. Maze

Instituto de Física, Pontificia Universidad Católica de Chile, Santiago, Chile and

Centro de Investigación en Nanotecnología y Materiales Avanzados (CIEN),

Pontificia Universidad Católica de Chile, Santiago, Chile

Carlos Cárdenas and Francisco Munoz

Center for the Development of Nanoscience and Nanotechnology (CEDENNA), Santiago, Chile and

Departamento de Física, Facultad de Ciencias, Universidad de Chile. Santiago, Chile

(Dated: July 18, 2023)

Most single photon emitters in hexagonal boron nitride have been identified as carbon substitutional defects, forming donor-acceptor systems. Unlike the most studied bulk emitters (*i.e.* color centers in diamond), these defects have no net spin, or have a single unpaired spin. By means of density functional calculations, we show that two non-adjacent carbon substitutional defects of the same type (*i.e.* C_B-C_B , and C_N-C_N), can have a triplet groundstate. In particular, one of such defects has a zero phonon line energy of 2.5 eV, and its triplet state is nearly 0.5 eV more stable than its singlet. The mechanism behind the destabilization of the singlet state is related to a larger electrostatic repulsion of a symmetric wave function in a charged lattice.

I. INTRODUCTION

The study and identification of the atomic defects associated with single photon emitters (SPEs) in hexagonal boron nitride (h-BN) is an active topic.[1–4] Excluding atomically engineered defects,[5, 6] experiments suggest C-based defects as SPEs.[7] So far, several substitutional C defects have been proposed. Those include monomers, different dimers (*i.e.* including non-adjacent atoms), trimers, arrangements of two close defects, and bigger substitutional clusters.[8–15] All these defects follow a similar logic, when a C atom replaces a B(N) atom, *i.e.* a C_B (C_N) defect, it behaves as a donor(acceptor). Larger defects, with an even number of defect atoms, are built to have as many donors as acceptors, and the occupied and empty states will have a sizable band gap (we will elaborate on this at the beginning of Sec. III). The case with an odd number of C atoms is similar, but with single uncompensated donor or acceptor, leading to a single extra energy level within the fundamental band gap. From this construction there exist only two possible spin configurations: (*i*) if the number of C atoms of the defect is even, the SPE has no net spin; (*ii*) if the number is odd, the SPE is paramagnetic with spin $S = \frac{1}{2}$. [8, 9]

To the best of our knowledge, there are only a few types of C-based proposals of high-spin SPEs, with $S \geq 1$. One combines a substitutional and an out-of-plane interstitial defect.[16] These defects offer an excellent example, beyond of the donor-acceptor logic, of a high-spin groundstate. The aforementioned defects have a set of zero phonon lines (ZPL) consistent with experimental results.[16] Nevertheless, interstitials defects have a large formation energy and small migration barriers,[17] and the natural occurrence of these defects should be

rather scarce, due to their high formation energy. The second is a combination of a vacancy with a substitutional C atom.[18] Again, the formation energy of these defects prevent them from being found in large concentrations.[17] The formation energy, H_f of a defect strongly depends on the chemical potential and Fermi energy, for single substitutional defects they are in the range $0 < H_f < 4.5$ eV. Excluding very specific combinations of Fermi energy and chemical potential, the H_f of vacancies or interstitials is at least 2 eV higher than in substitutions.[16, 17, 19]

The last proposal of SPEs with $S = 1$, introduced by Maciaszek *et al.*[17], is formed by four star-like substitutional C atoms: $C_B(C_N)_3$ and $C_N(C_B)_3$, they have a ZPL energy $\sim 2.0 - 2.2$ eV. These defects are an excellent example of pure substitutional C defects beyond from the standard donor-acceptor logic. However, these clusters only could be found in particular conditions (N-poor or N-rich), and with a rather low concentration (between two to three orders smaller than dimer or trimer defects).[17]

Experimentally, optically-detected magnetic resonance (ODMR) has been employed to detect the spin from SPEs. Most of the measurements are associated with the V_B^- defect.[20–22] However, there is evidence of other spinful defects,[7, 23–25] with a photoluminescence spectra consistent with pure substitutional C defects. Particularly, a recent study[26] has shown that a spin $S = 1$ or $S = \frac{3}{2}$ is required to explain their ODMR measurements.

In this article, we show that two substitutional C defects of the same type (*i.e.* $C_N C_N$ or $C_B C_B$) can have a triplet groundstate, which in most cases is just a few meV lower in energy than the singlet. However, there is a specific defect where the triplet state is nearly 0.5

eV more stable. We start by explaining our calculation methods in Sec. II. Then we show our results (Sec. III), starting with the simplest C_B and C_N defects and continuing with the dimer defects. Finally, in Sec. IV, we provide an explanation of our findings.

II. COMPUTATIONAL METHODS

Our central goal is to show that a triplet ground-state can be achieved with C-substitutional defects, even though it may seem counterintuitive at first glance. Then we will focus on the luminescent properties of the most interesting defect found. Our methodology reflects these goals, providing details about the accuracy of our calculations and measures to avoid possible methodological errors. Then, we explain the methodology used to calculate some properties: formation energy, ZPL energy, Huang-Rhys and Debye-Waller factors.

A. Calculation parameters and approximations

The calculations were performed with density functional theory (DFT), mostly by using the VASP package[27–30], but we also used the Gaussian code[31] in a few test calculations, as explained later in the text.

Regarding the settings of the VASP calculations (plane waves), the Perdew–Burke–Ernzerhof (PBE) and the Heyd–Scuseria–Ernzerhof (HSE) functionals were used.[32–34] The PBE functional gives a correct description of forces and geometries, however it has some shortcomings related to energies: (i) it underestimates the fundamental band gap of h-BN,[35] (ii) it underestimates the ZPL of C-based SPEs,[8] and (iii) it has problems representing the right distribution of localized states such as defect states. Conversely, the hybrid HSE functional gives quantitatively meaningful results, at a much higher computational cost.[36] One of the most important advantages of the HSE functional is the inclusion of Hartree-Fock exchange in the short-range part of the Coulomb interaction, which is important for accurately describing the difference in energy between states of different multiplicity. The HSE functional has a free parameter, defining the limit between short- and long-range of the Coulomb interaction. We used the popular so-called HSE06 version of the functional, *i.e.* the screening parameter is $\omega = 0.11$ bohr⁻¹ and the relative amount of Hartree-Fock exchange was 1/4.[34] Nevertheless, due to the decreased screening of 2D materials -such as h-BN- in some studies the value of the free parameter is changed to adjust the material’s band gap.[9] We do not expect a qualitative change by changing the form of the HSE functional (see Ref. [37] for a longer discussion on this topic).

Regarding the other parameters and settings of the calculations (VASP code), projector augmented-wave pseudopotentials were used.[38] A kinetic energy cutoff of 400

eV was employed, we tested a larger cutoff (650 eV) and it did not change the results significantly (see the Appendix). A single k-point (Γ) was used in the supercell calculations. PyProcar was employed for the analysis of the results,[39] and VESTA for the visualization.[40] The geometries were relaxed with PBE in both the ground and excited states. The relaxation with HSE06 of a specific defect, led to very similar results,[9] see Table V in the Appendix. The lattice parameter was set to 2.49 Å, the equilibrium value obtained with HSE06.

An especially tricky point could be the usage of periodic boundary conditions (PBC), at least for the systems with a small difference between the singlet and triplet states. All the PBC calculations shown here use a 8×8 supercell and the HSE06 functional. These calculations were tested at the PBE level with supercells ranging from 7×7 to 10×10 . The differences due to the supercell size were minimal. Convergence tests of the supercell size with HSE06 are given in the Appendix. It is worth remarking that the HSE06 functional should be even less dependent on the supercell size, since it provides a much better localization of the defect’s states.

To discard artifacts from the PBC, we used cluster models as explained in more detail in the Appendix. The shape of the clusters is critical for $C_N C_N$ clusters. Most cluster calculations were performed with VASP using the previous parameters, only the kinetic energy cutoff was increased to 500 eV, to better represent the finite size of the clusters. A few comparison calculations were performed with the Gaussian software, obtaining a good agreement between both codes. These calculations were done with the Gaussian 09.[31] For these calculations two double-Z basis set were used: 6-31+G(d) and cc-pVDZ.

B. Calculation of physical properties

The formation energy of a defect D in a charge state q is:

$$H_f(D, q) = E_{tot}(D, q) - E_{hBN} - n_C \mu_C - n_B \mu_B - n_N \mu_N + qE_F - E_{corr}, \quad (1)$$

where $E_{tot}(D, q)$ is the total energy of a supercell hosting the defect in the desired charge state, E_{hBN} is the energy of a pristine h-BN supercell, μ_i is the chemical potential of element i . n_i is the change in the number of atoms of element i , with respect to the pristine supercell. The Fermi energy E_F is set to zero at the valence band maximum. E_{corr} are corrections of large importance in charged defects.[41, 42] Since the defects we studied are neutral, $q = 0$, there is no need for an electrostatic correction.

The chemical potential represents a reservoir for the exchange of atoms. We took as reference for μ_B , μ_N , and μ_C , the energy per atom of bulk B, the N_2 molecule, and graphite, respectively. To simulate the limits of N-rich and N-poor conditions we followed the approach of Ref. [19].

The excited states were studied by means of the Δ SCF method.[43] The singlet groundstate is spin degenerate and its excitation is from the last occupied level to the first empty. For the triplet groundstate, the excitation with lowest energy also is from the last occupied level to the first empty, but the spin channel depends on the system: in $C_B C_B$ the transition takes place on the majority spin, while in $C_N C_N$ the excitation takes place on the minority spin.

The Huang-Rhys factor S measures the quantity of phonons participating in the ZPL transition. To obtain it, generalized coordinates q_k are needed.[44]

$$q_k = \sum_{\alpha} \sqrt{m_{\alpha}} (R_{e,\alpha i} - R_{g,\alpha i}) \Delta r_{k,\alpha i}, \quad (2)$$

where the indexes α , i and k denote atoms, Cartesian coordinates and vibrational modes, respectively. R_e and R_g are the positions in the excited and ground state, respectively. m_{α} is the mass of atom α , and Δr_k is the unitary vector of the k -th vibrational mode. Also, in this step we assumed that the vibrational modes for the ground and excited states are identical. In short, the above equation is a decomposition of the atomic rearrangement due to an optical excitation in the basis of the phonons.

The partial Huang-Rhys factor, S_k , quantifies the number of phonons of a given vibrational mode in the transition:

$$S_k = \frac{\omega_k q_k^2}{2\hbar}, \quad (3)$$

where ω_k represents the frequency of the phonon. Finally, the Huang-Rhys factor is obtained by adding all these partial factors, $S = \sum_k S_k$. On the other hand, the Debye-Waller factor measures the weight of the ZPL peak, w_{ZPL} , with respect to the total photoluminescence spectrum. Since there is no emission of phonons at the ZPL, $w_{ZPL} = e^{-S}$. [44]

III. RESULTS

A. The C_B and C_N defects

The simplest substitutional C defects are the replacement of a B or N atom by a carbon, they are denoted C_B and C_N , respectively, see Fig. 1. When neutral, these defects are candidates for SPEs within the visible range.[8, 9] In what follows we will focus only in the neutral cases. Both defects have groundstates within the fundamental band gap of h-BN. Each defect has a paramagnetic groundstate, $S = \frac{1}{2}$, and meanwhile C_B acts as a donor, with its last occupied level close to the conduction band, C_N acts like an acceptor with its first empty band near the middle of the band gap. If a C_B and a C_N are close enough, they form a dimer-like state, $C_B^+ C_N^-$, which is non-magnetic. It shows luminescence with a ZPL that varies with the separation between the C_N and C_B defects.[9]

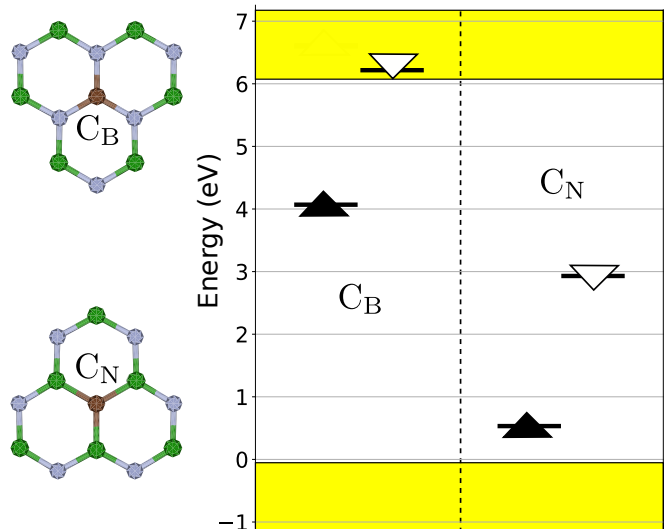


FIG. 1. (left panel) Scheme of the C_B and C_N defects. (right panel) Representation of the relevant defect levels close to the fundamental band gap. The different spins are denoted by different symbols, and the occupied/empty bands are marked by filled/empty symbols. The valence and conduction bands are marked by a yellow region. The B, N, and C atoms are colored green, gray, and brown, respectively.

TABLE I. Formation energy H_f of the different defects studied. They are reported for two extreme environments, N-poor and N-rich, as defined in Sec. II.

Configuration	H_f (eV)	
	N-poor	N-rich
$C_N C_N$ -2	3.82	9.02
$C_N C_N$ -3	3.82	9.02
$C_N C_N$ -4	3.83	9.03
$C_B C_B$ -2	8.47	3.27
$C_B C_B$ -3	8.49	3.29
$C_B C_B$ -4	8.47	3.27

B. The $C_B C_B$ and $C_N C_N$ dimers

The simplest way to avoid a donor-acceptor pair with a singlet groundstate is to consider two close defects of the same type, C_B or C_N . Up to a few lattice sites, their localized states overlap, and they can be considered as a single defect. See Fig. 2 for the geometry and labeling of the systems under study.

The formation energy, H_f , of the defects presented here is shown in Table I for two extreme conditions denoted as N-rich and N-poor, described in Sec. II. As expected, these values are similar to other C-based defects in h-BN, and their abundance should be determined by the actual environment.[17]

When both defect atoms are not too close (*i.e.* beyond nearest neighbors), their levels can be inferred up to some extent from the monomers, see Fig. 1 as reference, with two possible arrangements, the singlet and the triplet. The actual energy levels for a specific dis-

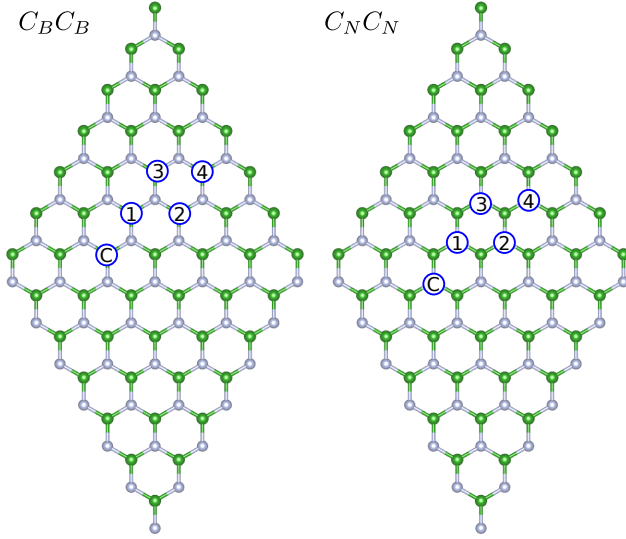


FIG. 2. Conformations of a $C_B C_B$ and $C_N C_N$ dimer as a function of the distance, up to three lattice constants apart. One substitutional C atom is kept fixed and the other is labelled according to their distance, in ascending order. For instance the $C_N C_N$ -3 dimer has one defect in the position marked ‘C’, and the other in the position marked ‘3’.

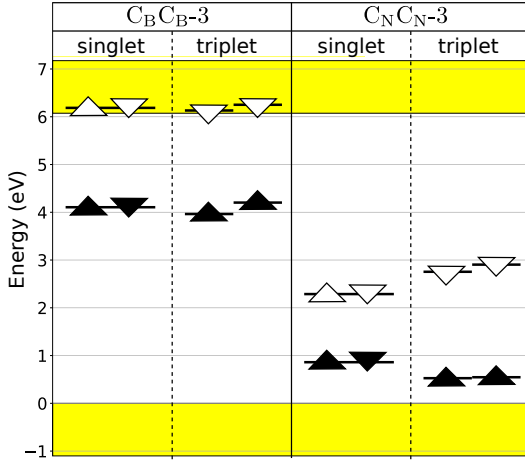


FIG. 3. Energy levels of the $C_B C_B$ -3 and $C_N C_N$ -3 defects, for the singlet and triplet states. The symbols are the same used in Fig. 1. The distance between both atoms is nearly 5 Å, see Table II.

tance are shown in Fig. 3. The visual inspection of the $C_B C_B$ -3 dimer shows no appreciable difference between the single and triplet arrangements. However, $C_N C_N$ -3 shows a much larger separation between the occupied and empty defect levels in the triplet, lowering the total energy. The different values of the defect levels as a function of the distance is shown in Fig. 4. The defects of the $C_B C_B$ family do not show any appreciable difference in the singlet states as a function of the distance. However, in the triplet there is an appreciable distance-dependent interaction for the same spin value. Just from inspect-

ing the energy levels the groundstate is not evident, *e.g.* the singlet and triplet have a comparable energy. The $C_N C_N$ defects show a similar pattern with the exception of $C_N C_N$ -3, which was already discussed and it will be explained in more detail in Sec. IV.

TABLE II. Energy difference $\Delta E^{(S-T)} = E_{\text{singlet}} - E_{\text{triplet}}$ for the studied cluster (*i.e.* a negative value implies a singlet groundstate). The values are obtained with the HSE06 functional, and using the PBE positions. The distances correspond to the singlet state, the values between parentheses correspond to the triplet state.

Label	distance (Å)	$\Delta E^{(S-T)}$ (meV)
$C_B C_B$ -2	4.32 (4.32)	-27
$C_B C_B$ -3	4.98 (4.98)	32
$C_B C_B$ -4	6.61 (6.61)	20
$C_N C_N$ -2	4.33 (4.35)	-44
$C_N C_N$ -3	5.02 (5.03)	482
$C_N C_N$ -4	6.61 (6.62)	19

The actual differences in total energy of all the systems studied are in Table II. In general, for closer defects ($C_X C_X$ -2) the singlet state is slightly more stable. For longer distances ($C_X C_X$ -4) the opposite is true. In the remaining case, $C_X C_X$ -3, for B defects, shows an intermediate behavior, with both configurations almost degenerate in energy. However, in $C_N C_N$ -3 the triplet is nearly 0.5 eV more stable than the singlet. Although this last result may seem strange at first glance, in the next section we will show that a lower energy for the triplet is to be expected. Additionally, an extensive set of convergence tests, including cluster models, is in the Appendix.

The defects $C_X C_X$ -3 share have in common a triplet groundstate. They can have an optical transition from the valence band to the unoccupied defect states. The zero phonon line (ZPL) of $C_N C_N$ -3 has energy $E_{ZPL} = 2.5$ eV, if the lowest energy level is involved in the transition. Its Huang-Rhys and Debye-Waller factors are $S = 1.37$ and $w_{ZPL} = 0.25$, respectively. In contrast, the defect $C_B C_B$ -3, has a ZPL energy $E_{ZPL} = 1.6$ eV, a much smaller electron-phonon, with $S = 0.67$ and $w_{ZPL} = 0.51$.

For the sake of comparison, experiments in h-BN, have found a myriad of SPEs, with wavelength covering the visible spectrum,[45] likely most of them are C-substitutional defects forming a donor-acceptor pair. Experimental values of the Huang-Rhys factor[10] are $S = 1.19 \pm 0.43$ ($w_{ZPL} = 0.33 \pm 0.13$). Also it is insightful to compare $C_X C_X$ -3 defects with the NV^- and SiV^0 defects found in bulk diamond, all of them with a triplet groundstate. The ZPL energy of the NV^- center is $E_{ZPL} = 1.94$ eV, and a very prominent phonon side-band, $S = 3.49$ ($w_{ZPL} = 0.03$).[46] The SiV^0 center has $E_{ZPL} = 1.67$ eV, and a remarkably small electron-phonon coupling, $S = 0.24$ ($w_{ZPL} = 0.79$).[47] In this respect, h-BN C-based defects have some clear advantages and drawbacks compared with their bulk diamond







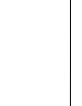

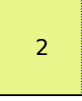
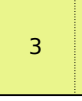
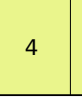
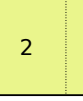
$C_B C_B$ singlet			$C_B C_B$ triplet			$C_N C_N$ singlet			$C_N C_N$ triplet		
											
											
											
2	3	4	2	3	4	2	3	4	2	3	4

FIG. 4. Energy levels of the $C_B C_B$ -X and $C_N C_N$ -X defects, the distance is specified in the lower part of each panel. The symbols are the same used in Fig. 1. The different color on the left and right sides is just a guide to the eye.

counterparts. First, a 2D material hosting the SPEs allows a much easier integration into devices, even more, there is unprecedented possibility of controlling the SPE by forming a van der Waals heterostructure.[48] Second, C-based SPEs in h-BN offer a ‘ultrabright’ stable luminescent signal, overcoming the signal of the NV^- and SiV centers.[49] We expect a similar behavior of the SPEs presented here. Third, the SPEs studied here have a small electron-phonon coupling, favoring long coherence times. However, the SiV center has an even smaller electron-phonon coupling, useful for quantum technologies. Fourth, there is a widespread problem to generate specific C-based SPEs in h-BN. We are aware of two reports of monochromatic SPEs in h-BN, blue[3] and yellow,[50] neither of them seems to be spin-active.

The energy difference $\Delta E^{(S-T)}$ of most $C_X C_X$ defects is smaller than room temperature (~ 26 meV), but larger than the critical temperature of liquid nitrogen (7 meV), which is easy to reach in experiments and make our predictions susceptible to experimental test. The triplet state in the defect $C_N C_N$ -3 should remain stable even near the dissociation temperature of h-BN (~ 3000 K).

IV. DISCUSSION

A simple model for the $C_X C_X$ defects is a two-electron molecule in an effective medium, similar to the H_2 molecule, but with extra terms in the Hamiltonian due to the h-BN lattice. The Hamiltonian is:

$$H = H_0 + \Delta V, \quad (4)$$

where H_0 is the standard Hamiltonian of a H_2 -like system,

$$H_0 = -\frac{\nabla_1^2}{2} - \frac{\nabla_2^2}{2} - \frac{1}{r_{1A}} - \frac{1}{r_{2B}} - \frac{1}{r_{1B}} - \frac{1}{r_{2A}} + \frac{1}{r_{12}} + \frac{1}{R_{AB}} \quad (5)$$

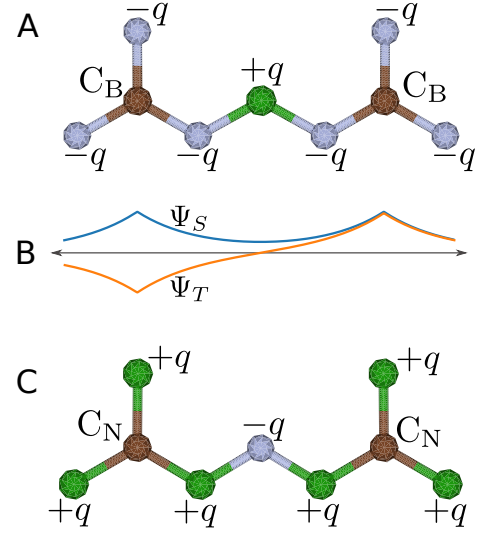


FIG. 5. Atomic environment for the $C_B C_B$ -3 (panel A) and $C_N C_N$ -3 (panel C) clusters. The charges centered at each atom are denoted by $\pm q$. The central panel (B) is a sketch of a typical singlet (Ψ_S , nodeless) and triplet (Ψ_T , with a node at its middle point) wave functions.

with the sub-indexes $\{1,2\}$ labelling both electrons, and the substitutional ions are denoted as $\{A,B\}$. The distances are $r_{\alpha\beta} = |r_\alpha - r_\beta|$. The contribution of the lattice to the $C_X C_X$ Hamiltonian can be modeled as an electrostatic-only contribution:

$$\Delta V = - \sum_{i \neq \{A,B\}} \frac{q_i}{r_{1i}} - \sum_{i \neq \{A,B\}} \frac{q_i}{r_{2i}}. \quad (6)$$

Here, q_i the effective charge of each site, which is negative (positive) for the N (B) atoms, see Fig. 5.

The solutions to Eq. 5 can be symmetric in the orbitals or in the spin, forming a singlet or a triplet, respectively. Without the lattice potential ($\Delta V = 0$), the relative energy of both states is given by *exchange* and *Coulomb*

integrals. The singlet state always has a lower energy, as it is well established [51].

Considering exponentially decaying states for the defect wave functions, the energy associated to ΔV will be similar for both the singlet and triplet for most lattice sites. This is because the localized wave function is relevant only for a few nearest neighbors, and the effects of having a (anti-) symmetric wave function are relevant only where the contribution of both states is non-negligible. However, there is a position of the lattice which is particularly relevant, at least for the $C_X C_X$ -3 defects. See Fig. 5, the atom at the midpoint between both C atoms is located in a region where the amplitude of the wavefunctions of the defect is not negligible. This atom is only ~ 2.5 Å apart from the C positions. Also, it can have a positive or negative net charge, which implies that this site is attractive for electrons in the case of the $C_B C_B$ -3 defect and repulsive in the case of $C_N C_N$ -3. If we label this atoms as M , the energy associated to this site is

$$V_M^\alpha \equiv \left\langle \Psi_\alpha \left| -\frac{q_M}{r_{1M}} - \frac{q_M}{r_{2M}} \right| \Psi_\alpha \right\rangle, \quad (7)$$

where $\alpha = \{S, T\}$ for a singlet or triplet state. For $C_B C_B$ -3, since the charge q_M is positive, a larger amplitude of $|\Psi_\alpha\rangle$ in this atom is favored. This is achieved in the nodeless singlet state, and V_M^α is such that $V_M^S < V_M^T < 0$. Contrary, for $C_N C_N$ -3, the potential due to the site M is repulsive for electrons, and the anti-symmetry of the triplet lowers the total energy: $0 < V_M^T < V_M^S$. Therefore, ΔV favors a triplet (singlet) for $C_N C_N$ -3 ($C_B C_B$ -3). The difference between the singlet and triplet wave function for $C_N C_N$ -3 is shown in Fig. 6, note the absence or presence of a central node. It is worth mentioning that with this simple analysis we only intend to provide an *ex post* explanation of our results. The simplicity of the model does not allow us to predict which will be the most stable state, the singlet or the triplet.

V. CONCLUSIONS

By means of DFT calculations we found that two substitutional C_N or C_B defects of the same type, have a triplet ($S = 1$) groundstate when both C atoms are sufficiently separated. In particular, when two C_N atoms are separated by two lattice parameters (≈ 5 Å, denoted $C_N C_N$ -3 in the article) the triplet state is lower in energy by ≈ 0.5 eV, compared with the singlet state. The ZPL associated with this defect is $E_{ZPL} = 2.53$ eV. In the remaining cases the energy difference between the triplet and singlet states is smaller than 0.05 eV.

The defect $C_N C_N$ -3 could explain the measured defects in h-BN with $S > \frac{1}{2}$. [7, 23, 25, 26] Since no vacancy is involved, they should have a large abundance [17]. Also, as pure substitutional C defects, they should exhibit the

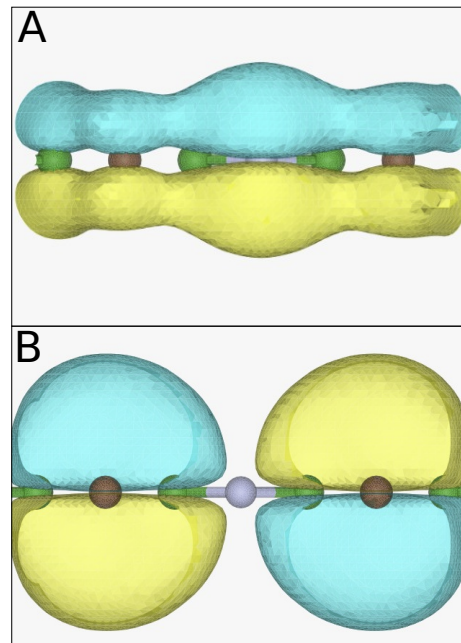


FIG. 6. Wave functions of one of the occupied defect states of the $C_N C_N$ -3 defect for the singlet (panel A) and triplet (panel B) states. The C-N-C atoms are shown. The wave functions corresponds to a PBE-level calculation.

typical phonon sideband (PSB) with lateral maximum shift 160 – 180 meV from the ZPL.[8].

On the other hand, the remaining non-adjacent $C_N C_N$ and $C_B C_B$ defects have a rather small energy difference between both the triplet and singlet state. Therefore, it could be possible to induce a switch between both states by means of an external field, or in a van der Waals heterostructure.

VI. COMPETING INTERESTS

The Authors declare no Competing Financial or Non-Financial Interests

VII. DATA AVAILABILITY

All input files are available from the corresponding author upon reasonable request.

VIII. AUTHOR CONTRIBUTIONS

F.P., C.C., N.V and F.M. run all the calculations. F.M. conceived the idea. F.M., J.R.M., and C.C. explained the stability of the triplet state. All authors discussed the results and contributed to the writing of the manuscript.

ACKNOWLEDGMENTS

This work was partially supported by Fondecyt Grants No. 1191353, 1220715, 1220366, and 1221512 by the Center for the Development of Nanoscience and Nanotechnology CEDENNA AFB180001, and from Conicyt PIA/Anillo ACT192023. This research was partially supported by the supercomputing infrastructure of the NLHPC (ECM-02).

Appendix A: Convergence and boundary conditions

The results from Table II, shows a drastic difference between one particular defect and the others. It is valid to ask whether these results are an artifact from the calculations or not. In this aspect we will show that for a large set of parameters the results do hold.

The first aspect to test is the role of the supercell size. We focus on the trends of the C_N-C_N defects with the HSE06 functional, since these defects show the abrupt changes. Table III shows the same behavior regardless of the size of the supercell. For the most separated defects, C_N-C_N-4 , the supercell influences the results in the range of a few meV.

TABLE III. Convergence respect to supercell size. The other parameters are given in Sec. II.

Label	Supercell	$\Delta E^{(S-T)}$ (meV)
C_N-C_N-2	6×6	-44
C_N-C_N-2	7×7	-44
C_N-C_N-2	8×8	-44
C_N-C_N-3	6×6	486
C_N-C_N-3	7×7	482
C_N-C_N-3	8×8	482
C_N-C_N-4	6×6	27
C_N-C_N-4	7×7	15
C_N-C_N-4	8×8	19

The completeness of the plane-wave basis is given by the kinetic energy cutoff, and in defect calculations it is critical to resolve localized states. We extensively tested the cutoff with the PBE functional (not shown here). Obtaining that a cutoff of 400 eV is good enough to have an accuracy of a few meVs. However, our results suggest that PBE is unable to correctly capture the localization of the defect's electron density. To check the accuracy of our results with a cutoff of 400 eV, we tested a cutoff of 650 eV for two defects with the most interesting/complex interplay between localization and electronic occupations. While at first glance it may be surprising that a cutoff of 400 eV is enough to describe localized defect states, this is the cutoff recommended in the pseudopotential to describe localized states, such as the h-BN bonds.

Another test is the effect of the atomic relaxation with HSE06, compared with the relaxation with PBE followed

TABLE IV. Effect of the kinetic energy cutoff. The other parameters are given in Sec. II.

Label	cutoff (eV)	$\Delta E^{(S-T)}$ (meV)
C_N-C_N-3	400	482
C_N-C_N-3	650	484
C_B-C_B-3	400	32
C_B-C_B-3	650	31

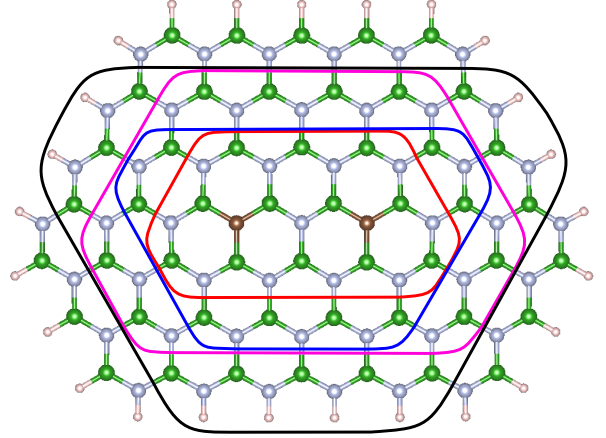


FIG. 7. Cluster models used in this test. The size (ignoring H atoms) of the clusters used is marked in the figure. The clusters are $B_{12}N_{11}C_2$ (inside red region), $B_{20}N_{16}C_2$ (inside blue region), $B_{28}N_{27}C_2$ (inside magenta region), $B_{39}N_{35}C_2$ (inside black region), $B_{50}N_{49}C_2$ (the full cluster in the figure). The smaller white atoms are H.

by a static calculation with HSE06. Again, we only tested the C_N-C_N defects. Table V shows a minor effect of the functional regarding the relative stability of the singlet/triplet states. This is because (i) PBE provides decent forces and positions, and (ii) the error in positions due to PBE is likely to be consistent (*e.g.* longer C-N bonds) and cancelled when measuring relative energies.

TABLE V. Effect of using the positions relaxed with PBE plus a HSE06 calculation without relaxation, compared to a full HSE06 relaxation. In both cases the results are calculated with a 7×7 supercell. The remaining parameters are given in Sec. II

Label	relaxation	$\Delta E^{(S-T)}$ (meV)
C_N-C_N-2	HSE06	-44
C_N-C_N-2	PBE	-44
C_N-C_N-3	HSE06	474
C_N-C_N-3	PBE	482
C_N-C_N-4	HSE06	16
C_N-C_N-4	PBE	15

The last test we made, is to use a cluster model to rule out artifacts from the PBC. The clusters are shown in Fig. 7. All the clusters are passivated with H atoms, and were created with pyPoscar[52]. The results are given in Table VI, and show a good agreement with supercell calculations. A strange trend is evident from the Ta-

ble VI with a minimum energy $\Delta E^{(S-T)}$ at $B_{28}N_{27}C_2$, and it increases for larger and smaller clusters. We interpret such behavior in terms of the localization of the defect wave functions, for smaller clusters it is spuriously localized, resulting in an increased interaction for both spin configurations. As the size of the system increases, the cluster boundaries become less relevant. However, it does not happen at the same rate. The triplet state is less localized, needing a larger cluster to avoid artifacts due to the finite boundaries. That extra interaction results in lower total energy of the triplet, in concordance with Table VI. Since we used a larger cutoff energy and

supercell size in these calculations, a perfect agreement with the results of periodic systems is unlikely.

TABLE VI. Cluster models for the defect $C_N C_N-3$. The shape of the cluster is shown in Fig. 7. The kinetic energy cutoff was set to 500 eV, the remaining parameters are given in Sec. II.

Cluster	$\Delta E^{(S-T)}$ (meV)
$B_{12}N_{11}C_2$	522
$B_{20}N_{16}C_2$	500
$B_{28}N_{27}C_2$	487
$B_{39}N_{35}C_2$	489
$B_{50}N_{49}C_2$	495

-
- [1] S. White, C. Stewart, A. S. Solntsev, C. Li, M. Toth, M. Kianinia, and I. Aharonovich, Phonon dephasing and spectral diffusion of quantum emitters in hexagonal boron nitride, *Optica* **8**, 1153 (2021).
- [2] R. J. P. Román, F. J. R. C. Costa, A. Zobelli, C. Elias, P. Valvin, G. Cassabois, B. Gil, A. Summerfield, T. S. Cheng, C. J. Mellor, P. H. Beton, S. V. Novikov, and L. F. Zagonel, Band gap measurements of monolayer h-BN and insights into carbon-related point defects, *2D Materials* **8**, 044001 (2021).
- [3] A. Gale, C. Li, Y. Chen, K. Watanabe, T. Taniguchi, I. Aharonovich, and M. Toth, Site-specific fabrication of blue quantum emitters in hexagonal boron nitride, *ACS Photonics* **9**, 2170 (2022).
- [4] M. Kianinia, Z.-Q. Xu, M. Toth, and I. Aharonovich, Quantum emitters in 2d materials: Emitter engineering, photophysics, and integration in photonic nanostructures, *Applied Physics Reviews* **9**, 011306 (2022).
- [5] M. Kianinia, S. White, J. E. Fröch, C. Bradac, and I. Aharonovich, Generation of spin defects in hexagonal boron nitride, *ACS Photonics* **7**, 2147 (2020).
- [6] X. Gao, S. Pandey, M. Kianinia, J. Ahn, P. Ju, I. Aharonovich, N. Shivaram, and T. Li, Femtosecond laser writing of spin defects in hexagonal boron nitride, *ACS Photonics* **8**, 994 (2021).
- [7] N. Mendelson, D. Chugh, J. R. Reimers, T. S. Cheng, A. Gottscholl, H. Long, C. J. Mellor, A. Zettl, V. Dyakonov, P. H. Beton, S. V. Novikov, C. Jagadish, H. H. Tan, M. J. Ford, M. Toth, C. Bradac, and I. Aharonovich, Identifying carbon as the source of visible single-photon emission from hexagonal boron nitride, *Nature materials* **20**, 321 (2021).
- [8] C. Jara, T. Rauch, S. Botti, M. A. L. Marques, A. Norambuena, R. Coto, J. E. Castellanos-Águila, J. R. Maze, and F. Munoz, First-principles identification of single photon emitters based on carbon clusters in hexagonal boron nitride, *J. P. Chem. A* **125**, 1325 (2021).
- [9] P. Auburger and A. Gali, Towards ab initio identification of paramagnetic substitutional carbon defects in hexagonal boron nitride acting as quantum bits, *Phys. Rev. B* **104**, 075410 (2021).
- [10] K. Li, T. J. Smart, and Y. Ping, Carbon trimer as a 2 eV single-photon-emitter candidate in hexagonal boron nitride: A first-principles study, *Phys. Rev. Materials* **6**, L042201 (2022).
- [11] M. Winter, M. H. E. Bousquet, D. Jacquemin, I. Duchemin, and X. Blase, Photoluminescent properties of the carbon-dimer defect in hexagonal boron-nitride: A many-body finite-size cluster approach, *Phys. Rev. Materials* **5**, 095201 (2021).
- [12] O. Golami, K. Sharman, R. Ghobadi, S. C. Wein, H. Zadeh-Haghighi, C. Gomes da Rocha, D. R. Salahub, and C. Simon, *abinitio* and group theoretical study of properties of a carbon trimer defect in hexagonal boron nitride, *Phys. Rev. B* **105**, 184101 (2022).
- [13] P. Huang, M. Grzeszczyk, K. Vaklinova, K. Watanabe, T. Taniguchi, K. Novoselov, and M. Koperski, Carbon and vacancy centers in hexagonal boron nitride, *arXiv preprint arXiv:2112.14906* (2021).
- [14] S. Li, A. Pershin, G. Thiering, P. Udvarhelyi, and A. Gali, Ultraviolet quantum emitters in hexagonal boron nitride from carbon clusters, *The Journal of Physical Chemistry Letters* **13**, 3150 (2022).
- [15] D. Amblard, G. D'Avino, I. Duchemin, and X. Blase, Universal polarisation energies for defects in monolayer, surface and bulk hexagonal boron nitride: A finite-size fragments gw approach, *arXiv preprint arXiv:2204.11671* (2022).
- [16] J. Bhang, H. Ma, D. Yim, G. Galli, and H. Seo, First-principles predictions of out-of-plane group iv and v dimers as high-symmetry, high-spin defects in hexagonal boron nitride, *ACS Applied Materials & Interfaces* **13**, 45768 (2021).
- [17] M. Maciaszek, L. Razinkovas, and A. Alkauskas, Thermodynamics of carbon point defects in hexagonal boron nitride, *Phys. Rev. Materials* **6**, 014005 (2022).
- [18] G. Cheng, Y. Zhang, L. Yan, H. Huang, Q. Huang, Y. Song, Y. Chen, and Z. Tang, A paramagnetic neutral cbvn center in hexagonal boron nitride monolayer for spin qubit application, *Computational Materials Science* **129**, 247 (2017).
- [19] L. Weston, D. Wickramaratne, M. Mackoito, A. Alkauskas, and C. G. Van de Walle, Native point defects and impurities in hexagonal boron nitride, *Phys. Rev. B* **97**, 214104 (2018).
- [20] N. Mathur, A. Mukherjee, X. Gao, J. Luo, B. A. McCullian, T. Li, A. N. Vamivakas, and G. D. Fuchs, Excited-state spin-resonance spectroscopy of v_B^- defect centers in hexagonal boron nitride, *Nature Communications* **13**

- (2022).
- [21] S. Baber, R. N. E. Malein, P. Khatri, P. S. Keatley, S. Guo, F. Withers, A. J. Ramsay, and I. J. Luxmoore, Excited state spectroscopy of boron vacancy defects in hexagonal boron nitride using time-resolved optically detected magnetic resonance, *Nano Letters* **22**, 461 (2022).
 - [22] P. Yu, H. Sun, M. Wang, T. Zhang, X. Ye, J. Zhou, H. Liu, C.-J. Wang, F. Shi, Y. Wang, and J. Du, Excited-state spectroscopy of spin defects in hexagonal boron nitride, *Nano Letters* **22**, 3545 (2022).
 - [23] N.-J. Guo, S. Li, W. Liu, Y.-Z. Yang, X.-D. Zeng, S. Yu, Y. Meng, Z.-P. Li, Z.-A. Wang, L.-K. Xie, R.-C. Ge, J.-F. Wang, Q. Li, J.-S. X. Xu, Y.-T. Wang, J.-S. Tang, A. Gali, and G.-C. Li, Chuan-Feng anfang Gup, Coherent control of an ultrabright single spin in hexagonal boron nitride at room temperature, *Nature Communications* **14**, 2893 (2023).
 - [24] N. Chejanovsky, A. Mukherjee, J. Geng, Y.-C. Chen, Y. Kim, A. Denisenko, A. Finkler, T. Taniguchi, K. Watanabe, D. B. R. Dasari, P. Auburger, A. Gali, J. H. Smet, and J. Wrachtrup, Single-spin resonance in a van der waals embedded paramagnetic defect, *Nature materials* **20**, 1079 (2021).
 - [25] W. Liu, N.-J. Guo, S. Yu, Y. Meng, Z.-P. Li, Y.-Z. Yang, Z.-A. Wang, X.-D. Zeng, L.-K. Xie, Q. Li, J.-F. Wang, J.-S. Xu, Y.-T. Wang, J.-S. Tang, C.-F. Li, and G.-C. Guo, Spin-active defects in hexagonal boron nitride, *Materials for Quantum Technology* **2**, 032002 (2022).
 - [26] H. L. Stern, Q. Gu, J. Jarman, S. Eizagirre Barker, N. Mendelson, D. Chugh, S. Schott, H. H. Tan, H. Sirringhaus, I. Aharonovich, and M. Atatüre, Room-temperature optically detected magnetic resonance of single defects in hexagonal boron nitride, *Nature communications* **13**, 1 (2022).
 - [27] G. Kresse and J. Hafner, Ab initio molecular dynamics for liquid metals, *Phys. Rev. B* **47**, 558(R) (1993).
 - [28] G. Kresse and J. Hafner, Ab initio molecular-dynamics simulation of the liquid-metal–amorphous-semiconductor transition in germanium, *Phys. Rev. B* **49**, 14251 (1994).
 - [29] G. Kresse and J. Furthmüller, Efficiency of ab-initio total energy calculations for metals and semiconductors using a plane-wave basis set, *Comput. Mater. Sci.* **6**, 15 (1996).
 - [30] G. Kresse and J. Furthmüller, Efficient iterative schemes for ab initio total-energy calculations using a plane-wave basis set, *Phys. Rev. B* **54**, 11169 (1996).
 - [31] M. J. Frisch, G. W. Trucks, H. B. Schlegel, G. E. Scuseria, M. A. Robb, J. R. Cheeseman, G. Scalmani, V. Barone, B. Mennucci, G. A. Petersson, H. Nakatsuji, M. Caricato, X. Li, H. P. Hratchian, A. F. Izmaylov, J. Bloino, G. Zheng, J. L. Sonnenberg, M. Hada, M. Ehara, K. Toyota, R. Fukuda, J. Hasegawa, M. Ishida, T. Nakajima, Y. Honda, O. Kitao, H. Nakai, T. Vreven, J. A. Montgomery, J. E. Peralta, F. Ogliaro, M. Bearpark, J. J. Heyd, E. Brothers, K. N. Kudin, V. N. Staroverov, R. Kobayashi, J. Normand, K. Raghavachari, A. Rendell, J. C. Burant, S. S. Iyengar, J. Tomasi, M. Cossi, N. Rega, J. M. Millam, M. Klene, J. E. Knox, J. B. Cross, V. Bakken, C. Adamo, J. Jaramillo, R. Gomperts, R. E. Stratmann, O. Yazyev, A. J. Austin, R. Cammi, C. Pomelli, J. W. Ochterski, R. L. Martin, K. Morokuma, V. G. Zakrzewski, G. A. Voth, P. Salvador, J. J. Dannenberg, S. Dapprich, A. D. Daniels, Farkas, J. B. Foresman, J. V. Ortiz, J. Cioslowski, and D. J. Fox, Gaussian 09, revision b.01 (2009).
 - [32] J. P. Perdew, K. Burke, and M. Ernzerhof, Generalized gradient approximation made simple, *Phys. Rev. Lett.* **77**, 3865 (1996).
 - [33] J. Heyd, G. E. Scuseria, and M. Ernzerhof, Hybrid functionals based on a screened coulomb potential, *J. Chem. Phys.* **118**, 8207 (2003).
 - [34] A. V. Krukau, O. A. Vydrov, A. F. Izmaylov, and G. E. Scuseria, Influence of the exchange screening parameter on the performance of screened hybrid functionals, *J. Chem. Phys.* **125**, 224106 (2006).
 - [35] N. Berseneva, A. Gulans, A. V. Krasheninnikov, and R. M. Nieminen, Electronic structure of boron nitride sheets doped with carbon from first-principles calculations, *Phys. Rev. B* **87**, 035404 (2013).
 - [36] P. Deák, B. Aradi, T. Frauenheim, E. Janzén, and A. Gali, Accurate defect levels obtained from the hse06 range-separated hybrid functional, *Phys. Rev. B* **81**, 153203 (2010).
 - [37] L. Muechler, D. I. Badrtdinov, A. Hampel, J. Cano, M. Rösner, and C. E. Dreyer, Quantum embedding methods for correlated excited states of point defects: Case studies and challenges, *Phys. Rev. B* **105**, 235104 (2022).
 - [38] G. Kresse and D. Joubert, From ultrasoft pseudopotentials to the projector augmented-wave method, *Phys. Rev. B* **59**, 1758 (1999).
 - [39] U. Herath, P. Tavazde, X. He, E. Bousquet, S. Singh, F. Muñoz, and A. H. Romero, Pyprocar: A python library for electronic structure pre/post-processing, *Comput. Phys. Commun.* **251**, 107080 (2019).
 - [40] K. Momma and F. Izumi, Vesta 3 for three-dimensional visualization of crystal, volumetric and morphology data, *Journal of applied crystallography* **44**, 1272 (2011).
 - [41] C. Freysoldt, B. Grabowski, T. Hickel, J. Neugebauer, G. Kresse, A. Janotti, and C. G. Van de Walle, First-principles calculations for point defects in solids, *Rev. Mod. Phys.* **86**, 253 (2014).
 - [42] M. H. Naik and M. Jain, Coffee: Corrections for formation energy and eigenvalues for charged defect simulations, *Computer Physics Communications* **226**, 114 (2018).
 - [43] Y. Jin, M. Govoni, G. Wolfowicz, S. E. Sullivan, F. J. Heremans, D. D. Awschalom, and G. Galli, Photoluminescence spectra of point defects in semiconductors: Validation of first-principles calculations, *Phys. Rev. Materials* **5**, 084603 (2021).
 - [44] A. Alkauskas, B. B. Buckley, D. D. Awschalom, and C. G. V. de Walle, First-principles theory of the luminescence lineshape for the triplet transition in diamond nv centres, *New Journal of Physics* **16**, 073026 (2014).
 - [45] D. Wigger, R. Schmidt, O. D. Pozo-Zamudio, J. A. Preuß, P. Tonndorf, R. Schneider, P. Steeger, J. Kern, Y. Khodaei, J. Sperling, S. M. de Vasconcellos, R. Bratschkitsch, and T. Kuhn, Phonon-assisted emission and absorption of individual color centers in hexagonal boron nitride, *2D Materials* **6**, 035006 (2019).
 - [46] C. Kurtziefer, S. Mayer, P. Zarda, and H. Weinfurter, Stable solid-state source of single photons, *Phys. Rev. Lett.* **85**, 290 (2000).
 - [47] S. Häußler, G. Thiering, A. Dietrich, N. Waasem, T. Teraji, J. Isoya, T. Iwasaki, M. Hatano, F. Jelezko, A. Gali, and A. Kubanek, Photoluminescence excitation spectroscopy of siv- and gev- color center in diamond, *New Journal of Physics* **19**, 063036 (2017).
 - [48] J. D. Caldwell, I. Aharonovich, G. Cassabois, J. H.

- Edgar, B. Gil, and D. Basov, Photonics with hexagonal boron nitride, *Nature Reviews Materials* **4**, 552 (2019).
- [49] T. T. Tran, K. Bray, M. J. Ford, M. Toth, and I. Aharonovich, Quantum emission from hexagonal boron nitride monolayers, *Nature nanotechnology* **11**, 37 (2016).
- [50] A. Kumar, C. Cholsuk, A. Zand, M. N. Mishuk, T. Matthes, F. Eilenberger, S. Suwanna, and T. Vogl, Localized creation of yellow single photon emitting carbon complexes in hexagonal boron nitride (2023), arXiv:2208.13488 [quant-ph].
- [51] W. Heitler and F. London, Wechselwirkung neutralen atome und homöopolare bindung nach der quantenmechanik, *Zeitschrift für Physik* **44**, 455 (1927).
- [52] pyposcar, <https://github.com/fvmunoz/pyposcar>.